INSTITUTE OF PHYSICS PUBLISHING JOURNAL OF PHYSICS D: APPLIED PHYSICS

J. Phys. D: Appl. Phys. **36** (2003) A172–A176 PII: S0022-3727(03)60704-7

Kinetics of the field induced commensurate to ferro-electric phase transition in thiourea

K-D Liss[1], M Kaiser[2], J Hlinka[3], F Denoyer[4], R Hock[5], R Currat[6]

[1] Division for Neutron and X-Ray Scattering, GKSS-Forschungszentrum, Postfach 1160, D-21494 Geesthacht, Germany
[2] European Synchrotron Radiation Facility, BP 220, F-38043 Grenoble Cédex, France
[3] Institute of Physics AS CR, Na Slovance 2, CZ-182 21 Prague 8, Czech Republic
[4] Laboratoire de Physique des Solides, Bat. 510, Université Paris-Sud, F-91405 Orsay Cédex, France
[5] Lehrstuhl für Kristallographie und Strukturphysik, D-91054 Erlangen, Germany
[6] Institut Laue-Langevin, BP 156, F-38042 Grenoble Cédex, France

E-mail: liss@kdliss.de

Received 14 September 2002
Published 28 April 2003
Online at stacks.iop.org/JPhysD/36/A172

Abstract

The paper examines the kinetics of the electric field induced, first-order transition from the commensurate to the ferro-electric phase in thiourea ($SC(NH_2)_2$) at 170 K. The satellite reflection from the modulated phase, locked in with a wave vector $\boldsymbol{q} = 1/9\boldsymbol{b}^*$ disappears when the phase transition is induced by a static electric field E_c along the $\boldsymbol{a}$-axis. In order to study the kinetics of the phase transition, an oscillating electric voltage of rectangular shape was applied to the sample and photon events were acquired separately for ON- and OFF-field half-periods. Results received in a series of measurements at different amplitudes between 0 and 500 V and frequencies between 0.125 and 512 Hz lead to the conclusion that a slow and a fast relaxation time play a role for the OFF → ON and the ON → OFF transitions, respectively. Further, the highest frequency at which the phase transformation still follows the switching of the electric field depends linearly on the applied field amplitude. A qualitative explanation of the experimental results is given in terms of nucleation and growth of specific ferro-electric domains.

1. Introduction

Stroboscopic methods have been established recently to access dynamic and kinematical aspects in solid state physics which are too slow for spectroscopic studies such as inelastic neutron and x-ray scattering [1–3]. Brilliant x-ray beams from modern synchrotron radiation sources are a powerful basis to further develop them. Radiation damage and heating of the sample may be a drawback at conventional energies [4] while photons above 100 keV interact so weakly with the sample that this problem disappears. An alternative is to employ stroboscopic neutron diffraction as it has been realized in an experiment by Eckold *et al* [5].

Structural changes at phase transitions are well examined by x-ray diffraction methods, while little is known about the timescale over which these rearrangements take place. Electrically induced rather than temperature or pressure driven phase transitions are of particular experimental interest since they can be switched rapidly compared to the relaxation times of the system. Moreover, temperature changes are extremely slow and repeated pressure changes by means of ultrasonic transducers [6] or laser impacts as necessary for stroboscopic acquisition would heat the system, which then runs out of experimental control. Because of these reasons, an electric field seems to be the most convenient driving parameter for real-time measurements. Related investigations can be found even on constrained systems like, e.g. thin films of $BaTiO_3$ as investigated by Zolotoyabko *et al* [1] and references therein.

For our study, we have chosen the electrically induced phase transition between the modulated and ferro-electric

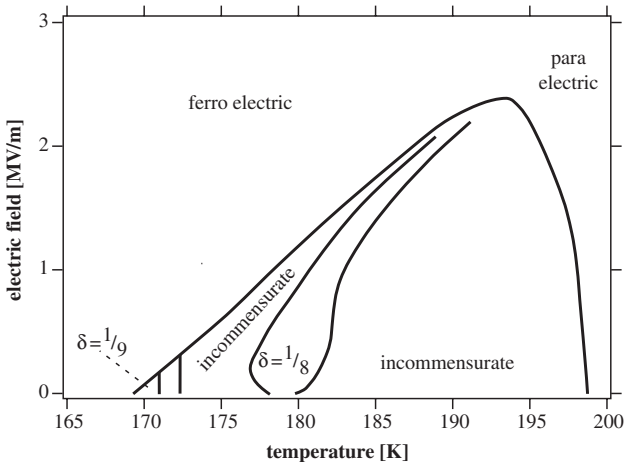

Figure 1. Phase diagram of thiourea ($SC(NH_2)_2$) after [8]. A series of modulated phases exists between the para-electric and ferro-electric phases at low electric field strengths. Our results were obtained at constant temperature of 170 K, but under applied electric field $E > E_c$, which facilitates the phase transition from the modulated phase with $\delta = 1/9$ to the ferro-electric phase. The critical field is 50 KV m^{-1}.

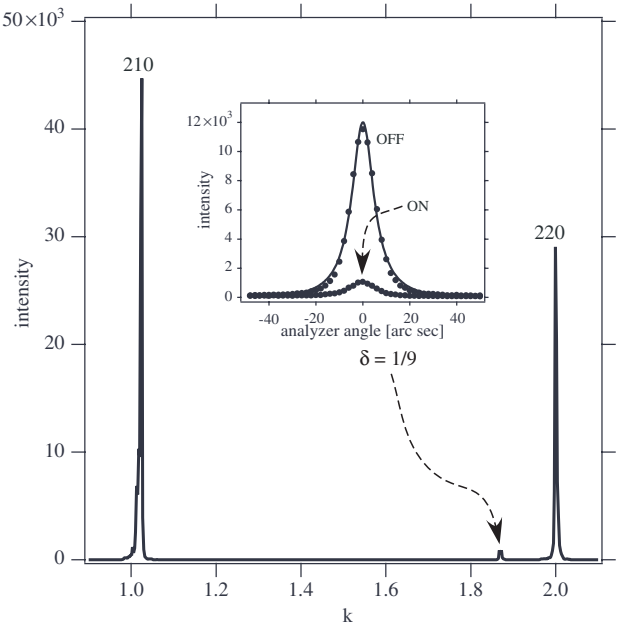

Figure 2. Reciprocal space scan with a triple axes diffractometer along the Miller index k. A satellite reflection appears at $T = 170$ K with $k = 2 - 1/9$. The insert shows an analyser scan through the satellite peak without (OFF) and with a high enough electric field (ON) showing a considerably reduction of the diffracted intensity. Integrated intensities are evaluated by fitting the data to Lorentzian curves.

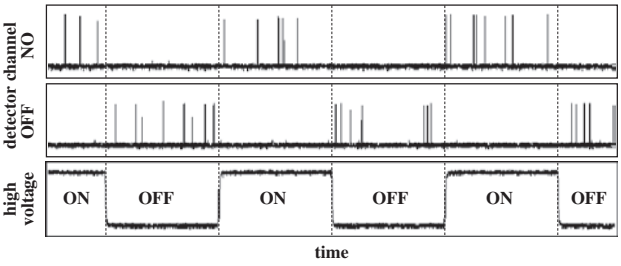

Figure 3. Snapshot of the oscilloscope screen showing the oscillation of the applied high voltage and the gating of the detector channels for the OFF and ON half-periods. The spikes are the photon events which are counted during the intervals when respective voltage levels are applied.

phases in thiourea, $SC(NH_2)_2$. The structure and physical properties have been rather well characterized and described elsewhere [7–9] and reveal a complicated phase diagram in electric field E–temperature T-coordinates. According to figure 1, there exists a region of modulated phases with a wave vector ($\boldsymbol{q} = \delta \boldsymbol{b}^*$) between $T = 199$ and 171 K. With descending temperature, the parameter δ shrinks continuously from $0.141 > \delta > 1/8$, passes the $\delta = 1/8$ lock-in point at $T = 179$ K and diminishes further to lock-in with $\delta = 1/9$ at $172\,\text{K} > T > 171$ K. These temperatures depend on hysteresis effects. Below the first-order transition temperature of $T = 169$ K the modulated phase disappears in favour of a ferro-electric one. The latter can be achieved as well at any temperature in the range of the modulated phases by applying a high enough electric field $E > E_c$ along the orthorhombic $\boldsymbol{a}$-axis. Our interest was to start from the $\delta = 1/9$ phase, switching the field above E_c.

2. Experimental set-up

A cube-shaped sample with edges of approximately 3 mm along the orthorhombic axes of the crystal lattice has been cut from a crystal grown by a slow evaporation method from a methyl alcohol solution. The polished $\boldsymbol{a}$-faces were plated by 100 nm AuPd electrodes and contacted by means of 0.05 mm thick silver wires. The crystal was mounted into a Teflon holder with the $\boldsymbol{c}$-axis pointing up and put on the tip of the sample stick placed into an orange helium cryostat. The leads were linked to a coaxial cable and connected to the voltage supply unit. An alternating voltage was applied to the sample. Its amplitude could be varied between 0 and 500 V and its frequency between 0 (static measurements) and 512 Hz.

The diffraction experiment was performed on the triple axes diffractometer at the high energy beamline ID15A at the ESRF [10]. Oxygen precipitated silicon 311 monochromator and analyser crystals were used in Laue geometry. In particular, the analyser crystal was necessary to distinguish between the spiky intensity distribution from the mosaic spread of the imperfect sample and a satellite reflection from the modulated phase. One of the reflection curves is given in figure 2 as an analyser scan at $T = 170$ K in the $\delta = 1/9$ phase. With no field, it shows a clear intensity profile which tends to disappear under an electric field well above E_c. We attribute the residual intensity due to field inhomogeneities at the crystal edges.

The detector signal was gated for the oscillating field acquisition such that photon events arriving during the field OFF and ON half-periods were stored into two different channels (see figure 3). Since we realized the existence of a hysteresis effect depending on the field history applied to the sample, we implemented an empirical erasing cycle at 500 Hz and 500 V for 15 s with the aim to 'return' the system into a starting condition fairly comparable to a very long field OFF relaxation.

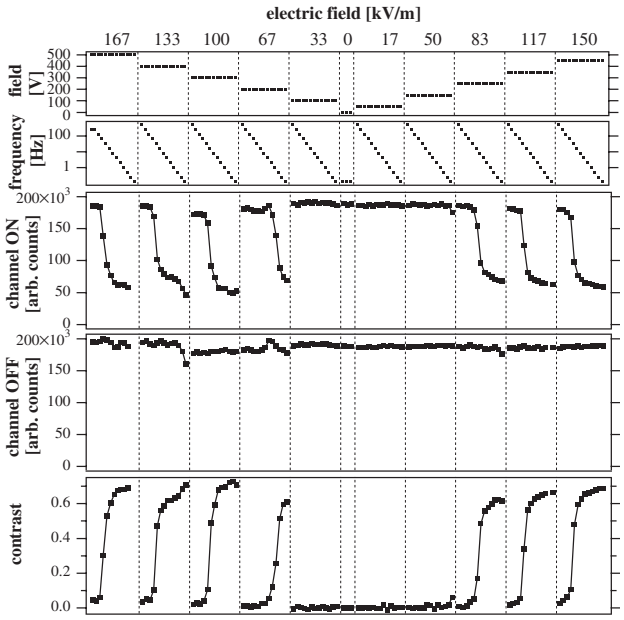

Figure 4. Integrated intensities for the ON and OFF half-periods (3rd and 4th panels) and contrast (5th panel) as a function of electric field and frequency parameters (1st and 2nd panels). The values for the OFF channels are constant while the ON channels vary on the field parameters. The contrast tends to zero for field amplitudes below the threshold and for high frequencies where the system cannot follow the oscillation.

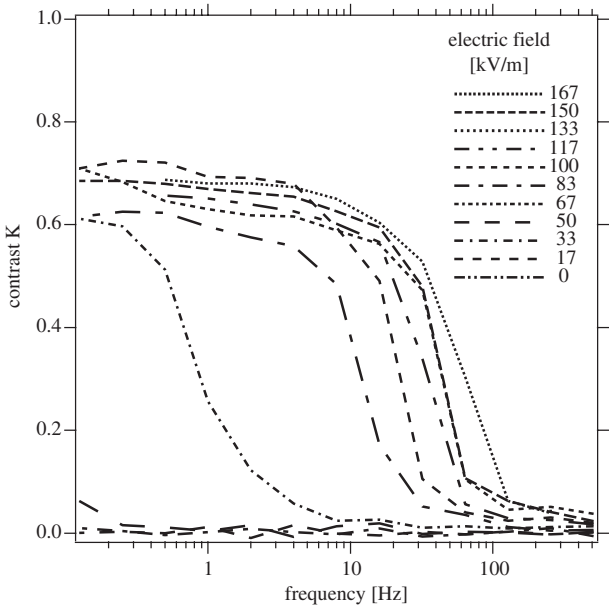

Figure 5. Contrast curves as a function of frequency for different field amplitudes. The system cannot follow the field oscillations at high frequencies. The critical frequency where the system fails to follow the electric field variation depends on the field amplitude.

3. Experimental data

A program was run to apply voltages of {500, 400, 300, 200, 100, 0, 50, 150, 250, 350, 450 V, each oscillating with {512, 256, 128, 64, 32, 16, 8, 4, 2, 1, 0.5, 0.25, 0.125} Hz at constant temperature of 170 K. These parameters are given in the first and second panels of figure 4. The integrated intensities I_{ON} and I_{OFF} of the satellite reflection corresponding to the $\delta = 1/9$ phase are given in the third and fourth panel for both ON and OFF half-periods, respectively. It makes sense to define a kind of contrast

$$K = \frac{I_{OFF} - I_{ON}}{I_{OFF}} \tag{1}$$

which is plotted in the last panel of figure 4. It is highest when I_{ON} and I_{OFF} represent the static behaviour at very low frequencies, while it tends to zero when the system does not follow the field amplitude at high frequencies. Somewhere in-between these two regimes, there exists a critical frequency ν_c at which the system ceases to follow the oscillation. These are the frequency positions when the contrast approaches its minimum value in the diagrams. We stress, that only the ON channels show intensity changes which depend on the voltage and frequency parameters, while all OFF channels remain of constant intensity. Figure 5 compares directly the contrast curves as a function of frequency for the different voltages. For strong enough fields, K tends to zero for high frequencies and to a maximum value under static conditions. The phase transition cannot be reached at all for fields $E < E_c$, which is demonstrated by vanishing K for all investigated frequencies.

4. Results

As expected, we observe the static values of the contrast for very low frequencies as the stationary limit. On the other hand, one could naively await the response to a time averaged field E_{avg} for high frequencies which would behave like a static field. Then, the transition would only take place if $E_{avg} > E_c$, which clearly is not the observation. Instead, the intensity of the OFF-channels does not change as a function of the voltage and frequency parameters. This means, there exist two different relaxation times for opposite directions of the phase transformation, a slow and a much faster one (which we did not access in this experiment) when the field is switched ON or OFF, respectively.

The second result is the behaviour of the critical frequency at which the phase transition sets on as a function of the applied field and is consistent with earlier observations of this system [4]. The solid markers in figure 6 show the data points where relaxation takes place, i.e. where the contrast K deviates from its high-frequency limit. The smaller open circles represent the region, in which the system does not follow the high-frequency field. The border line between these regions depends linearly on the applied field amplitude. Just above the critical field strength it tends to zero (0.125 Hz for $E = 50\,\mathrm{kV\,m^{-1}}$) and increases to 128 Hz for the highest applied field of $167\,\mathrm{kV\,m^{-1}}$. Therefore, in this case for $E \geqslant E_c$ we can write

$$\nu_c = C(E - E_c) \tag{2}$$

with $E_c \approx 50\,\mathrm{kV\,m^{-1}}$ and $C = 109\,\mathrm{m\,s^{-1}\,kV^{-1}}$.

5. Discussion

We would like to consider the possibility that the transition to the ferro-electric phase can proceed by a process known

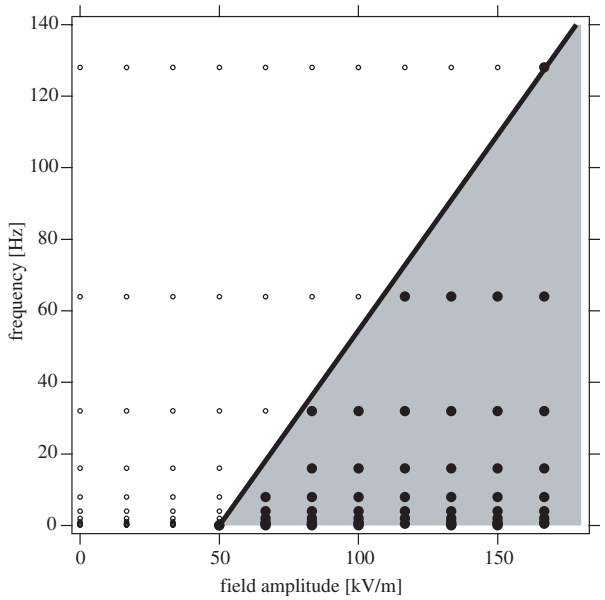

Figure 6. Phase diagram in amplitude–frequency space. The open and solid markers represent all experimental points where data have been taken. For the solid dots alone the contrast differs from its high-frequency limit. The linear behaviour sets on above the threshold field of 50 KV m^{-1} and spans over the whole frequency range from 0.125 to 128 Hz.

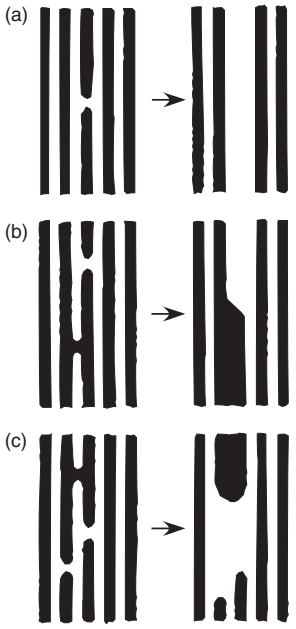

Figure 7. Illustration of the mechanism of domain pattern coarsening by nucleation and growth of antistripples. Antistripples are areas of switched domains which earlier belonged to the opposite polarization. (*a*) Simple nucleation and coarsening to a stripe of triple width, (*b*) nucleation in two adjacent, opposite polarized domains leading to a step in the structure and (*c*) nucleation of three adjacent antistripples forming a more complicated pattern (after [11]).

as nucleation and growth of 'antistripples' as demonstrated in figure 7 [11]. Such processes were thoroughly observed, e.g. in coarsening of the lamellar domain pattern in $NaNO_2$ crystals thermally quenched to the ferro-electric phase [12]. The modulated phase of thiourea can be visualized as the ferro-electric phase with a dense regular lamellar domain structure, the lamellae being perpendicular to the modulation wave vector. Therefore it seems natural to speculate about the same type of coarsening on the scale of the modulation. Actually, the same assumption was invoked to explain the formation of the lamellar habitus of the observed domain structure itself [13].

Obviously, the dynamical behaviour of the 'wide' antistripples in the quenched ferro-electric phase should differ from that of the micro-antistripples formed during the field induced transition itself. The lamellar 'micro-domains' forming the modulated phase have either preferred or non-preferred orientation with respect to the applied bias electric field. Therefore, the growth of only one kind of micro-antistripples is supported by the field. The nucleus of such preferred micro-antistripple is nothing more than a hole-like region of preferred polarization inside of one not-preferred lamellar domain, which connects the two adjacent lamellar domains of the preferred polarity. As the extend of reversed area increases, the perturbed lamellar domain gradually disappears at the expense of a newly formed, three times wider lamellar domain of preferred polarity.

Let us stress that there are no domain wall drifts along the direction perpendicular to the lamellae in this picture. In the case of micro-antistripples, such a drift would lead to an unacceptable change of modulation wave vector in the adjacent regions of the almost perfect modulated phase. On the other hand, one can expect that the boundary of the sufficiently large preferred micro-antistripple moves in the directions perpendicular to the modulation wave vector with a constant velocity proportional to the electric field, and can be thus characterized by an intrinsic mobility μ as in the case of the usual ferro-electric domain wall. At zero field, the modulated structure corresponds to the lowest energy state so that the micro-antistripples may tend to shrink. This fact can be taken into account by assuming an effective internal field E_i acting on the domain wall in a way to restore the homogenous modulated state. The velocity of preferred antistripple boundary may thus read as

$$v = \mu(E - E_i). \tag{3}$$

Since, in a weakly damped, oscillating system, the velocity is proportional to the frequency, this linear dependence is in excellent agreement with the experimental results and equation (2).

It is important to stress that the micro-antistripple mechanism is by its nature relevant only to the phase transformation towards the ferro-electric state. Indeed, the nuclei of the modulated phase has to look much more 'classical', since it has to contain several equidistant micro-domain boundaries defining the modulated period. Such classical nuclei were in fact observed for example in simulations reported in [14]. In this way, the micro-antistripple mechanism can provide a sufficient basis for qualitative understanding of the striking difference between the backward and forward transformation velocities.

Further investigations are necessary to clarify this interesting problem. First of all, the stroboscopic acquisition should employ thousands of channels rather than two to access as well the fast relaxation time. In order to study in full detail the behaviour of the critical frequency more sophisticated voltage supplies can be envisaged which allow us to switch

between two different mono- or bipolar levels rather than between an ON and an OFF state. The temperature dependent measurements will prove that we are in the appropriate region of the phase diagram. Although we exclude temperature changes in consistence with Eckold et al [5] due to high frequency heating, this point should be clarified in detail.

The presented method has been adapted for the first time to high energy x-rays and applied to study the kinetics of a phase transition. Particularly, its high angular resolution is a great advantage as compared to neutron scattering experiments [5] in this field. In fact, we can envisage to study in future fine details on the diffraction pattern like the lock-in transition around the 1/8 modulated and the incommensurate phases.

Acknowledgments

We are grateful to B Brezina and P Vanek from Institute of Physics AS CR in Prague for growing thiourea crystals used in this study. This work has been partially supported by the Grant Agency of the Czech Republic (Project No 202/99/D066) and by fully supported beam time at the ESRF.

References

[1] Zolotoyabko E, Quintana J P, Hoerman B H and Wessels B W 2002 Fast time-resolved x-ray diffraction in $BaTiO_3$ films subjected to a strong high-frequency electric field *Appl. Phys. Lett.* **80** 3159–61

[2] Liss K-D, Magerl A, Hock R, Waibel B and Remhof A 1998 The investigation of ultrasonic fields by time resolved x-ray diffraction *Proc. SPIE* **3451** 117–27

[3] Liss K-D, Magerl A, Hock R, Remhof A and Waibel B 1997 Towards a new (Q, t) regime by time-resolved x-ray diffraction: ultra-sound excited crystals as an example *Europhys. Lett.* **40** 369–74

[4] Komori S, Hayase S and Terauchi H 1989 The rate process of the field-induced modulated-ferroelectric phase transition in thiourea *J. Phys.: Condens. Matter* **1** 3789–99

[5] Eckold G, Hagen M and Steigenberger U 1998 Kinetics of phase transitions in modulated ferroelectrics: Time-resolved neutron diffraction from Rb2ZnCl4 *Phase Transitions* **67** 219–44

[6] Liss K-D, Magerl A, Remhof A and Hock R 1997 Ultrasound induced gradient crystals observed by high energy x-rays *Acta Crystallogr.* A **53** 181–6

[7] Simonson T, Denoyer F and Currat R 1985 Structure of the modulation in thiourea. I. Symmetry properties *J. Phys.* **46** 2187–95

[8] Boudot C, Mangin J and Durand D 1987 Phase transitions in H-thiourea under electric-field *Phase Transitions* **9** 163–72

[9] Shiozaki Y 1990 Organic crystals *Ferroelectrics and Related Substances* ed E Nakamura (Berlin: Springer) p 193–5

[10] Liss K-D, Royer A, Tschentscher T, Suortti P and Williams A P 1998 On high resolution reciprocal space mapping with a triple crystal diffractometer for high energy x-rays *J. Synchrotron Radiat.* **5** 82–9

[11] Hamano K, Zhang J, Abe K, Mitsui T, Sakata H and Ema K 1996 Dynamical process of domain pattern coarsening in ferroelectric sodium nitrite I. Microscopic observation *J. Phys. Soc. Japan* **65** 142–8

[12] Yamada Y 1981 Dynamical structure analysis and its application to the study of the non-equilibrium state of $NaNO_2$ *Ferroelectrics* **35** 51–6

[13] Hlinka J, Ishibashi Y and Nagaya T 1998 Formation of an amorphous domain pattern in type-II incommensurate ferroelectrics *J. Phys. Soc. Japan* **67** 3999–4001

[14] Nagaya T and Ishibashi Y 1996 Growth kinetics of domain structures under applied fields in crystals with an incommensurate phase—the case of no Lifshitz invariant *J. Phys. Soc. Japan* **65** 1812–19